journal

J. Am. Ceram. Soc., 78 [2] 479-86 (1995)

Processing of Silicon Carbide–Mullite–Alumina Nanocomposites

Yoshio Sakka*

National Research Institute for Metals, 2-1, Sengen-1, Tsukuba, Ibaraki 305, Japan

Donald D. Bidinger* and Ilhan A. Aksay*

Department of Chemical Engineering and Princeton Materials Institute, Princeton University, Princeton, New Jersey 08544-5263

Nanocomposite materials in the form of nanometer-sized second-phase particles dispersed in a ceramic matrix have been shown to display enhanced mechanical properties. In spite of this potential, processing methodologies to produce these nanocomposites are not well established. In this paper, we describe a new method for processing SiC–mullite–Al_2O_3 nanocomposites by the reaction sintering of green compacts prepared by colloidal consolidation of a mixture of SiC and Al_2O_3 powders. In this method, the surface of the SiC particles was first oxidized to produce silicon oxide and to reduce the core of the SiC particles to nanometer size. Next, the surface silicon oxide was reacted with alumina to produce mullite. This process results in particles with two kinds of morphologies: nanometer-sized SiC particles that are distributed in the mullite phase and mullite whiskers in the SiC phase. Both particle types are immersed in an Al_2O_3 matrix.

I. Introduction

CERAMIC-MATRIX nanocomposites have been receiving increasing attention largely due to their significantly enhanced mechanical properties, low-temperature densification, machinability, and superplastic behavior.[1–3] For instance, in the pioneering studies of Niihara and his colleagues, fracture strengths as high as 1.5 GPa and toughnesses as high as 7.5 $MPa \cdot m^{1/2}$ have been reported in systems where nanometer-sized SiC was dispersed in Al_2O_3, MgO, Si_3N_4, and mullite matrices.[3,4] Niihara classified nanocomposites into two general categories.[3] One category consists of composites of only nanometer-sized grains. The other consists of composites where nanosized particles are distributed within the intra- and/or intergrain regions of micrometer-sized grains. The main advantage in using nanocomposites of the first category is that they can be shaped by superplastic deformation, whereas the main advantage of the nanocomposites of the second category is their enhanced high-temperature stability against grain coarsening. In this paper, we deal with the processing of the second type of nanocomposite with a novel reaction sintering method.

Nanocomposites produced by Niihara's group have been formed mainly by using composite powders mixed on the nanometer scale by conventional milling of micrometer-sized powders. Although the mechanisms of size reduction to nanometer scale and the entrapment of particles within each other are not clearly understood, this conventional milling approach has certainly been effective in processing nanocomposites with unique properties despite the fact that milling of powders generally results in contamination or reproducibility problems. Alternatively, chemical vapor deposition (CVD) has also been successfully used to process similar nanocomposites.[3] However, as stated by Niihara,[3] the use of CVD to fabricate large and complex-shape components is not suitable for mass production.

We propose the use of reaction sintering as a more economical and reliable method for producing nanocomposites. In this study, we chose the SiC–mullite–Al_2O_3 system because it has been shown that SiC–mullite, SiC–Al_2O_3, and mullite–SiC systems have excellent mechanical properties.[3–6] Our procedure consists of the three steps shown in Fig. 1.[7] First, we consolidated micrometer-sized SiC and Al_2O_3 powders homogeneously through colloidal consolidation (slip casting), which is known to be an excellent processing route for improved mechanical behavior.[8,9] Second, partial oxidation treatment was conducted to oxidize the surface of the SiC particles to SiO_2 and thus to reduce the size of the SiC particles to nanometer size. Finally, we reacted the surface oxide and Al_2O_3 to produce mullite. As we illustrate in the following sections, the advantages of this method are that (1) the reduction of the inclusion phase to nanoscale can be achieved without milling and (2) because of a volume increase during reaction sintering, the sintering shrinkage is low.

II. Experimental Procedure

The α-Al_2O_3 powder used in this study was Sumitomo Chemical's (AKP-50) high-purity alumina ($\geq$99.995%) with a mean particle diameter of 0.21 μm and a specific surface area of 9.5 m^2/g. Two types of β-SiC powders were used: Superior Graphite's HSC059 containing C (0.85 wt%), Si (0.03), N (0.21), and O (0.80) as major impurities, and Mitsui Toatsu's MSC-20 containing SiO_2 (0.11 wt%) as a major impurity. Figure 2 shows TEM photographs of the two powders. Superior Graphite's powder is relatively coarse (indicated as SiC(C)) with a wide particle size distribution, a mean particle diameter of 0.56 μm, and a specific surface area of 15.0 m^2/g. Mitsui Toatsu's powder is finer (indicated as SiC(F)) with a narrow particle size distribution, a mean particle diameter of 0.15 μm, and a specific surface area of 21.3 m^2/g.

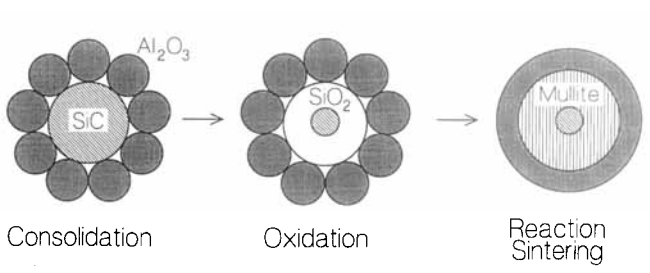

Fig. 1. Schematic illustration of the process steps used to produce nanocomposites by reaction sintering.

M. Sacks—contributing editor

Manuscript No. 194576. Received May 12, 1993; approved March 23, 1994.
Supported by the U.S. Air Force Office of Scientific Research under Grant No. AFOSR-F49620-93-1-0259.
*Member, American Ceramic Society.

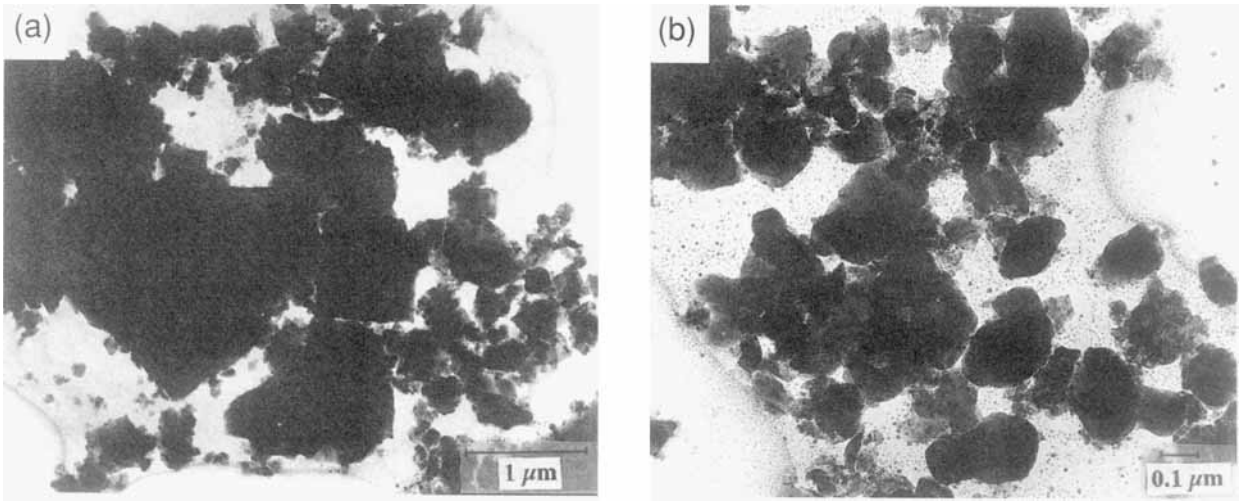

Fig. 2. TEM photographs of (a) SiC(C) and (b) SiC(F) powders.

The zeta potential of the two SiC powders in suspension was obtained by the Smoluchowski equation[10] from the electrophoretic mobility (Otsuka Electronics ELS-800 and Bel Japan Zetasizer 4) determined on diluted suspensions containing 0.01*M* NaCl (or 0.01*M* KCl) to control ionic strength. The pH was adjusted using NaOH (or KOH) and HCl.

Stable colloidal suspensions with a solid content of 45 vol% were prepared electrosterically in distilled water with an NH_4 salt of poly(methacrylic acid) (PMAA, Darvan C) at pH 10 as described in the next section. NH_4OH was used to adjust the pH. After ultrasonic vibration (Sonic Materials Vibracell 600W Unit, Danbury, CT) was applied for 10 min to facilitate the dispersion of the powder agglomerates, the suspension was stirred using a magnetic stirrer for over 12 h at room temperature. Degassing of the suspension was achieved in a bell jar connected to a vacuum pump. A colloidal consolidation technique employing a gypsum mold was used to consolidate the colloidal particles. The compacts were then dried overnight at 100°C.

Thermogravimetric analysis (TGA; TGA7 thermogravimetric analyzer, Perkin-Elmer, Norwalk, CT) was conducted to determine the oxidation level of SiC by weight increase. The dried compacts were put into a platinum pan and heated to predetermined soak temperatures at a heating rate of 10°C/min in a stream of air.

After partial oxidation treatment in air, reaction sintering was conducted in an alumina crucible in a stream of Ar using a graphite furnace at a heating rate of 25°C/min and a cooling rate of 5°C/min. The densities of the green compacts and the sintered bodies were measured by the Archimedes method using kerosene or distilled water, respectively. The pore channel size distribution of the compacts was determined by mercury porosimetry.[11,12] The pore channel size distribution was obtained using standard values for the mercury surface energy (0.48 N/m) and the contact angle (140°). Phase analysis was conducted by X-ray diffraction (XRD; X-ray diffractometer, Philips Electronic Instruments, Inc, Mahwah, NJ) using Ni-filtered Cu$K\alpha$ radiation. Sintered samples were polished down to a 1-μm surface finish with diamond paste and then thermally etched at 1450°C for 20 min in an Ar atmosphere. The resulting microstructures were evaluated by scanning electron microscopy (SEM; Philips 515 scanning electron microscope) and transmission electron microscopy (TEM; Philips 300 transmission electron microscope).

III. Results and Discussion

(1) Consolidation Process

In preparing colloidal suspensions, controlling the interactions between particles has a significant influence on the stability of a suspension. In our system, an electrosteric stabilization approach was preferred over an electrostatic one since it was not possible to disperse both SiC and Al_2O_3 equally well at the same pH level. When only electrostatic dispersion was used, SiC dispersed best under basic conditions since the zeta potential is higher in basic solutions, as seen in Fig. 3, whereas Al_2O_3 dispersed best under acidic conditions.[13–15] Consequently, an NH_4 salt of PMAA was used as an electrosteric stabilizer (0.4 g/m^2)[14,15] to improve the stability of Al_2O_3 under basic conditions so that a low-viscosity composite suspension could be prepared at pH 10.

Figure 4 shows pore channel size distributions of the Al_2O_3–15SiC(C) compacts consolidated by the colloidal consolidation of the suspensions with different values of pH. A green compact with a narrow pore channel size distribution with small pores could be obtained by adjusting the pH.

During colloidal consolidation of binary suspensions, a key problem is the segregation of particles due to either gravitational[11,12,16] or thermodynamic phase separation[17,18] effects. The best solution for minimizing particle segregation is to prepare the suspensions as highly concentrated as possible.[11,12,16–19] In our system, to check if segregation and/or phase separation occurred, the green densities and X-ray intensity ratios along the perpendicular axis of both Al_2O_3–15SiC(C) and Al_2O_3–15SiC(F) compacts (approximately 3.5 cm height) were measured. Because these displayed similar values within experimental error, it was concluded that significant segregation and/or phase separation did not occur while using a 45 vol% solid suspension. As shown in Figs. 5 and 6, relatively

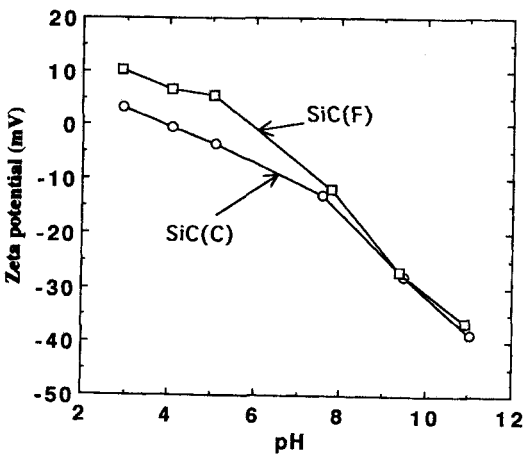

Fig. 3. Plots of zeta potential vs pH for SiC(C) and SiC(F).

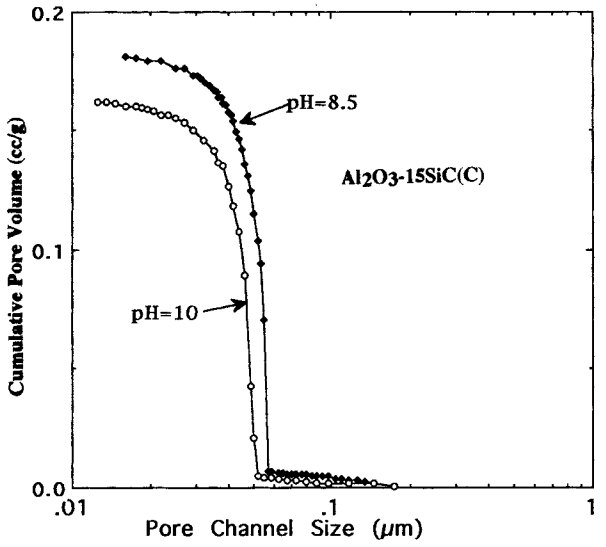

Fig. 4. Pore channel size distributions of the Al_2O_3–15SiC(C) compacts consolidated by the colloidal consolidation of the suspensions with different values of pH.

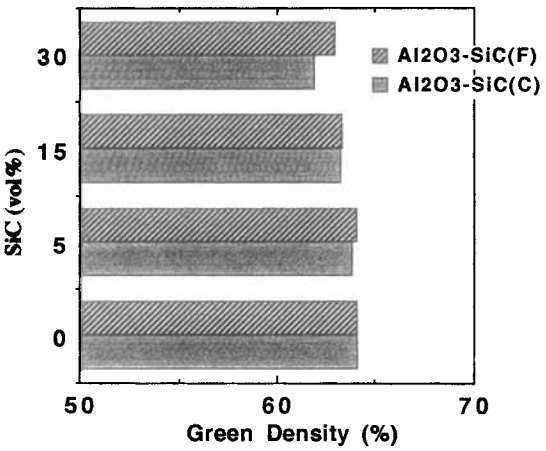

Fig. 5. Green densities of the colloidally consolidated composites with various amounts of SiC(C) and SiC(F) powders.

high green densities (Fig. 5) and narrow pore channel size distributions (Fig. 6) obtained with all of these compacts were also an indication of the consolidation of the particles without significant segregation.

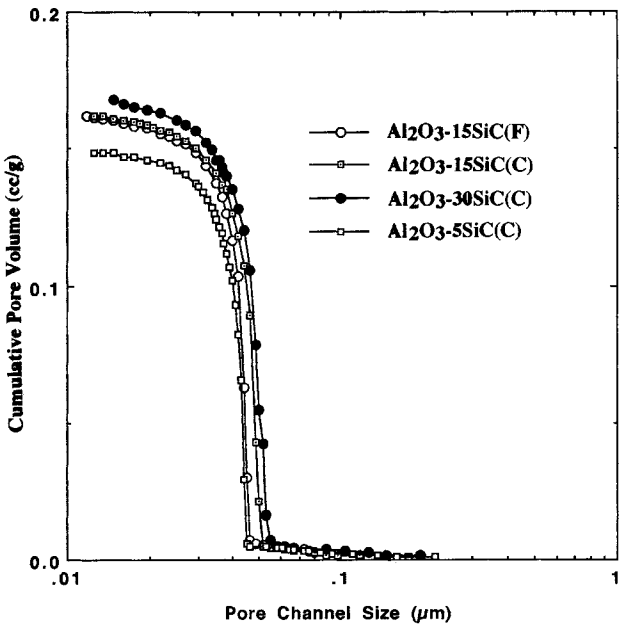

Fig. 6. Pore channel size distributions of the colloidally consolidated composites with various amounts of SiC(C) and SiC(F) powders.

(2) Oxidation Process

The typical weight losses and/or gains when heating Al_2O_3–15SiC(F) and Al_2O_3–15SiC(C) at a heating rate of 10°C/min are shown in Fig. 7. Upon heating to 700°C weight loss was observed in three regions for the Al_2O_3–15SiC(C) sample: in the first region (up to 300°C), the second (around 350°C), and the third (around 650°C). To determine the origin of the weight loss, a TGA experiment on the Al_2O_3 compact after colloidal consolidation was conducted. By comparison with the weight loss of Al_2O_3–15SiC(C) and Al_2O_3, it is concluded that the first weight loss was due to desorption of water and the second is due to decomposition of the surfactant. Although slight weight loss of Al_2O_3 was observed due to the chemically bonded water (i.e., hydroxy groups) in the temperature range of 400–1000°C, the weight loss was different from that of the third region. Temperature-programmed desorption measurement[20,21] of SiC(C) powder in oxygen atmosphere was conducted, where the evolved gases were monitored with a quadrupole spectrometer. The evolution of CO and CO_2 was observed in the third region. Therefore, in the third region the weight loss was mainly due to the evolution of carbon oxide from carbon impurity. In the case of Al_2O_3–15SiC(F), the third region was not observed because carbon was not a major impurity in the SiC(F). Above 700°C for Al_2O_3–15SiC(C) and above 500°C for Al_2O_3–15SiC(F), the weight loss reached a maximum value

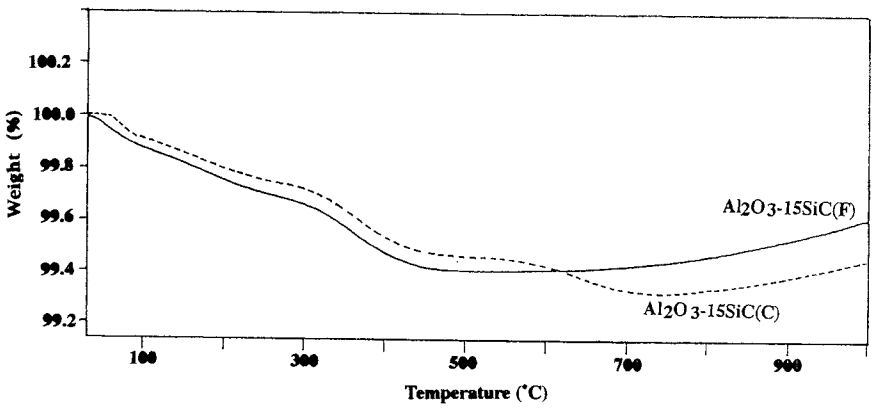

Fig. 7. TGA curves of colloidal consolidated compacts of Al_2O_3–15SiC(C) and Al_2O_3–15SiC(F) at a heating rate of 10°C/min in a stream of air.

and, because of the onset of SiC oxidation, a weight gain was observed at higher temperatures. The plateau value at the maximum weight loss was used as the reference point to approximate the fraction of silica that formed as an oxidation product on the surface of the SiC particles.

The size of the SiC core particles was controlled by determining the fraction of SiC oxidized during heat treatment. Figure 8 shows the weight gain and oxidation fraction. Because of its finer particle size, the oxidation fraction of the SiC(F) system is higher than that of the SiC(C) system. The oxidation behavior of SiC powder in this temperature range is believed to be the following passive oxidation reaction:[22]

$$SiC + 2O_2 \longrightarrow SiO_2 + CO_2 \quad (1)$$

The oxidation reactions at 1400°C are depressed by comparison with those at 1300°C, especially for the SiC(C) system, as seen in Fig. 8. This phenomenon may be due to the significant sintering occurring simultaneously with the oxidation reaction at 1400°C. Therefore, partial oxidation treatments were conducted below 1400°C. Many authors have reported that oxidation of SiC powders in various oxidizing atmospheres follows parabolic reaction rate kinetics.[22–27] The oxidation fraction can be represented by the following Jander's equation:[28]

$$1 - (1 - f)^{1/3} = (kt)^{1/2} \quad (2)$$

where f is the oxidation fraction, t is the reaction time, and k is the rate constant. As shown in Fig. 9, when $1 - (1 - f)^{1/3}$ is plotted versus the square root of time, a linear variation is observed at low temperatures (1000–1200°C) and also within the initial stages of higher temperature oxidation treatments,

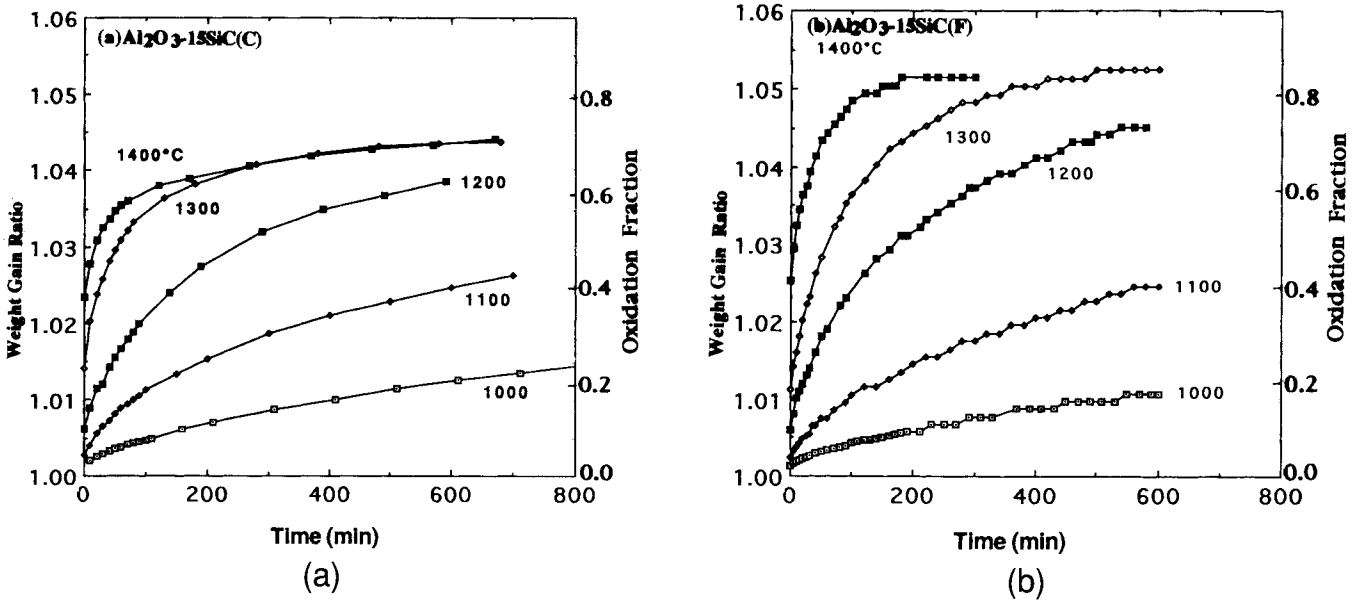

Fig. 8. Weight increase ratio (left-hand side) and oxidation fraction (right-hand side) of (a) Al_2O_3–15SiC(C) and (b) Al_2O_3–15SiC(F) composites during isothermal holding in a stream of air.

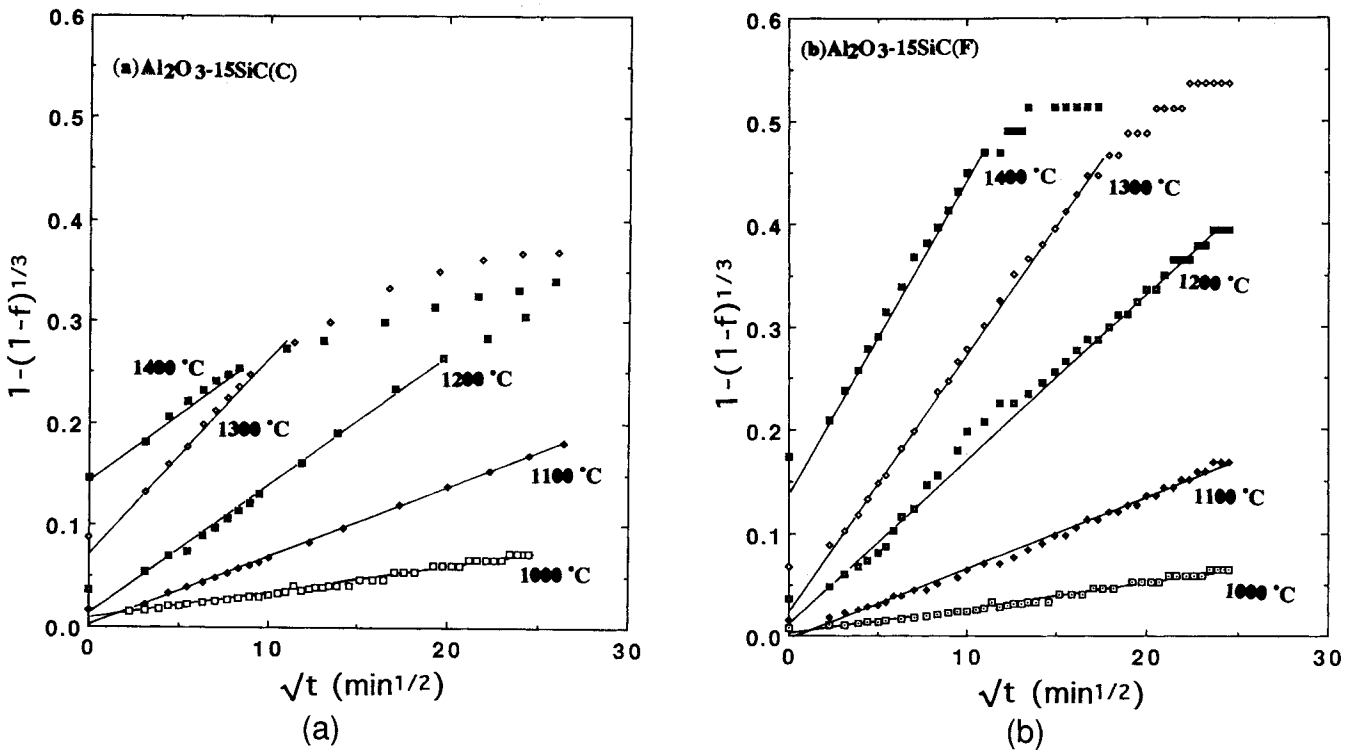

Fig. 9. Relationship between square root of time and $1 - (1 - f)^{1/3}$ for (a) Al_2O_3–15SiC(C) and (b) Al_2O_3–15SiC(F) composites during isothermal holding in a stream of air.

suggesting that oxidation is rate limited by a diffusion process. Using Eq. (2), we can calculate the rate constants at every temperature. Arrhenius plots of the rate constants in the temperature range of 1000–1300°C are shown in Fig. 10. The activation energies of Al_2O_3–SiC(F) and Al_2O_3–15SiC(C) are 256 and 216 kJ/mol, respectively. Activation energies reported in the literature vary from 134 to 498 kJ/mol.[22–27] The large amount of scatter has been attributed to the different types of materials (powder, polycrystal, and single crystal) with varying concentrations of impurities, which can alter the oxidation kinetics significantly. In our case, the activation energies are close to the activation energy of the ionic oxygen diffusion in vitreous silica (298 kJ/mol)[29] but not to that of the molecular oxygen diffusion (113 kJ/mol).[30] Therefore, the present oxidation reaction seems to proceed via ionic oxygen diffusion through a silica film.

Figure 11 shows the X-ray diffraction patterns of Al_2O_3–15SiC oxidized at 1300°C for 5 h in air. The decrease in the amount of SiC and the gain in the amount of SiO_2 (cristobalite and amorphous phase) can be seen from the figure. In the case of Al_2O_3–15SiC(F) (Fig. 11(b)), the SiC peak was broader and

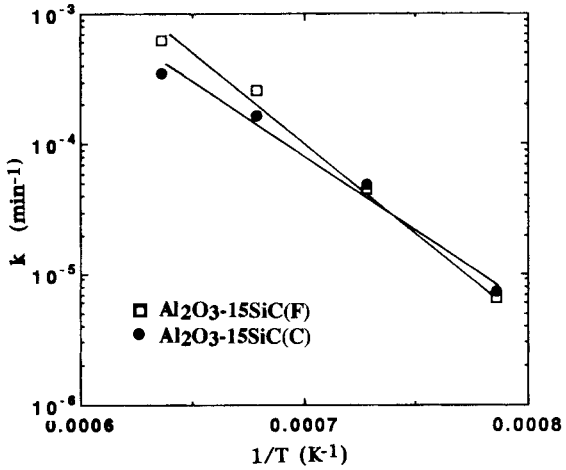

Fig. 10. Arrhenius plots of the rate constants.

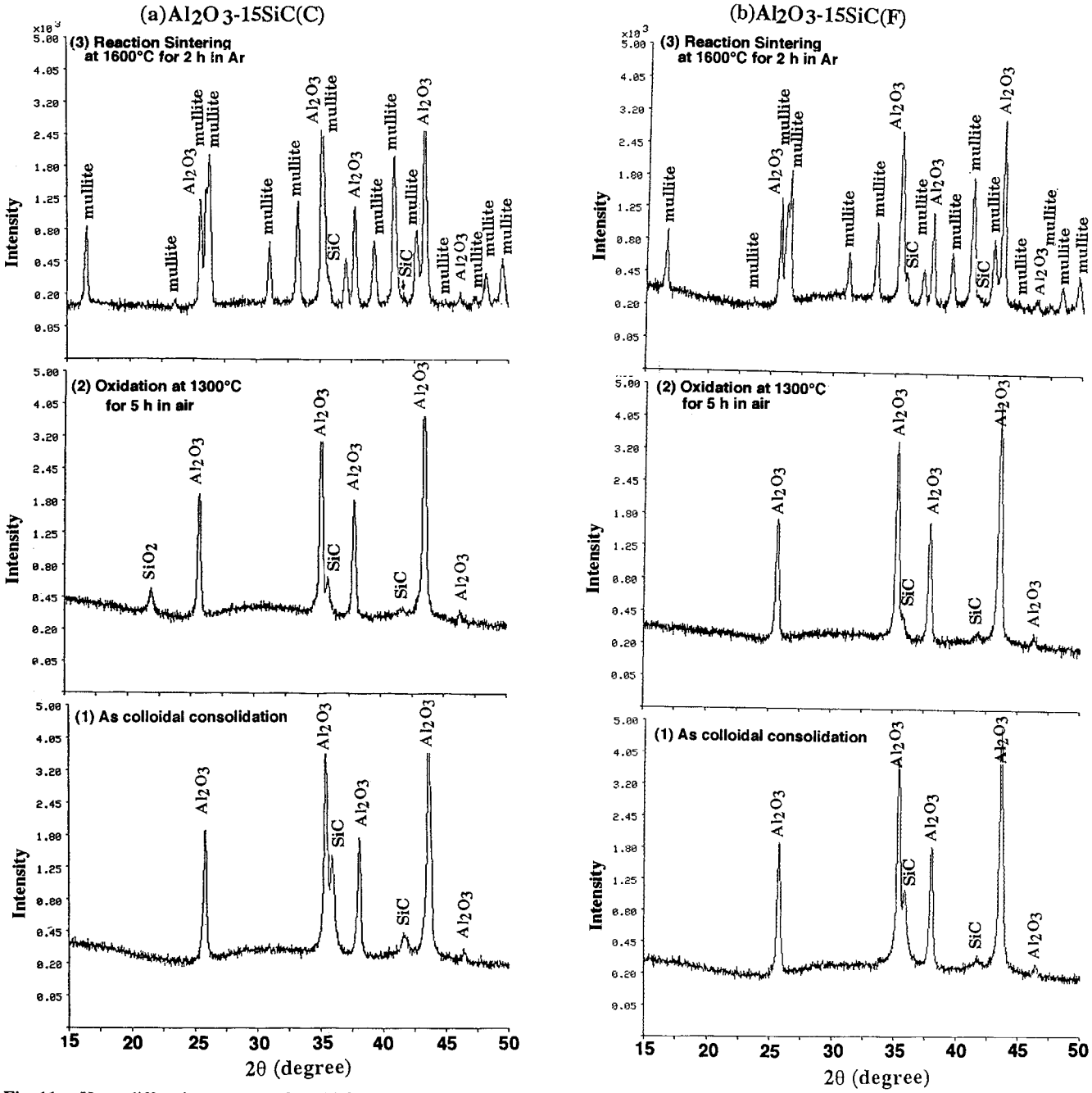

Fig. 11. X-ray diffraction patterns of (a) Al_2O_3–15SiC(C) and (b) Al_2O_3–15SiC(F): (1) as colloidal consolidation, (2) after oxidation at 1300°C for 5 h in air, and (3) after reaction sintering at 1600°C for 2 h in Ar.

the cristobalite phase was not observed after partial oxidation treatment. It is important to note that a large quantity of cristobalite is not preferred since cristobalite causes micro- and macrocracking during its β- to α-cristobalite polymorphic phase transformation during cooling.

(3) Reaction Sintering and Microstructure

Comparison of the X-ray diffraction patterns in Fig. 11 confirms the premise of this study that the SiO_2 phase would form as an oxidation product and be consumed to form mullite during the final stage heat treatment in Ar. In calculating the theoretical densities of the compacts, two types of volume expansion had to be considered.[31] Volume expansion of SiC upon oxidation is 107% and formation of stoichiometric mullite from the reaction of $3Al_2O_3$ and $2SiO_2$ results in a volume increase of ~5% assuming that the densities of Al_2O_3, SiO_2, and mullite are 3.99, 2.33, and 3.16 g/cm^3, respectively. The theoretical densities were determined by the following equation:

$$\rho = [V_s\rho_s + (1 - V_s)\rho_A]W/k \quad (3)$$

where ρ_s and ρ_A are the theoretical densities of SiC and Al_2O_3, respectively, V_s is the volume fraction of SiC, and W is the oxidation weight increase ratio. k is a factor controlled by the composition and the respective volume expansions:

$$k = \frac{fV_s(2.07 \times 1.05 - 1)}{1 + (1 - f)V_s} + 1 \quad (4)$$

where f is the oxidation fraction of SiC.

The effects of the oxidation conditions on the sintered densities are shown in Fig. 12. Note that when the oxidation fraction exceeded 40% (by comparison of Figs. 8 and 12), sintered densities above 95% were obtained by sintering at 1600°C for 2 h in an Ar atmosphere. In contrast, the densities of the samples with no partial oxidation treatment were very low. The presence of amorphous silica after surface oxidation of SiC accelerates the sintering significantly. A possible explanation for this is the lowering of porosity due to volume expansion during the oxidation of SiC. Although amorphous silica forms only on the SiC particles, the possibility of enhanced densification due to its transient presence needs further investigation.[32,33] As expected, the final composite densities show a slight decrease as the initial SiC content is increased (Fig. 13).

Figure 14 shows a SEM micrograph of a polished and etched Al_2O_3–15SiC(C) sample that was oxidized at 1300°C and sintered at 1600°C. At this resolution, although small second-phase inclusions are observed, it is not obvious whether these inclusions extend to the nanoscale range. In TEM characterization of the composites, two types of nanoscale inclusions were observed (Fig. 15). In the first type (Fig. 15(a)), nanometer-sized SiC particles were observed as inclusions within a mullite matrix as confirmed by energy dispersive X-ray spectroscopy (EDS), where the SiC particles were seen as dark spots. In the second type (Fig. 15(b)), mullite whiskers were observed within the SiC grains, again as confirmed by EDS analysis.

These morphologies are explained as follows. When Mitsui Toatsu's fine SiC is used, the surface of the SiC is oxidized uniformly and nanometer-sized SiC particles remain in the mullite matrix as illustrated in Figs. 1 and 15(a). In contrast, since Superior Graphite's SiC powders are coarser and are produced by milling, the powders may have grain boundaries and cracks

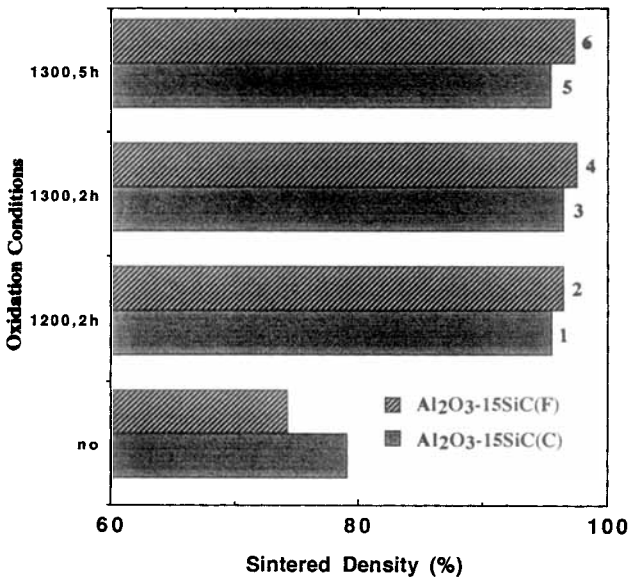

Fig. 12. Effect of oxidation conditions on the densities of the compacts sintered at 1600°C for 2 h in Ar. Calculated compositions of the produced nanocomposites are as follows:

Sample no.	Composition (vol%)		
	Al_2O_3	Mullite	SiC
1	63.5	27.6	8.9
2	61.0	31.0	8.0
3	52.3	42.1	5.6
4	51.3	43.5	5.2
5	48.2	47.3	4.5
6	43.5	53.6	2.9

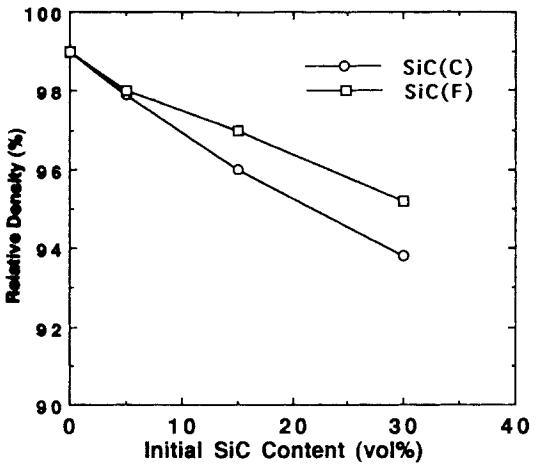

Fig. 13. Effect of initial SiC contents on density after an initial oxidation at 1300°C in air and then a final sintering at 1600°C for 2 h in Ar.

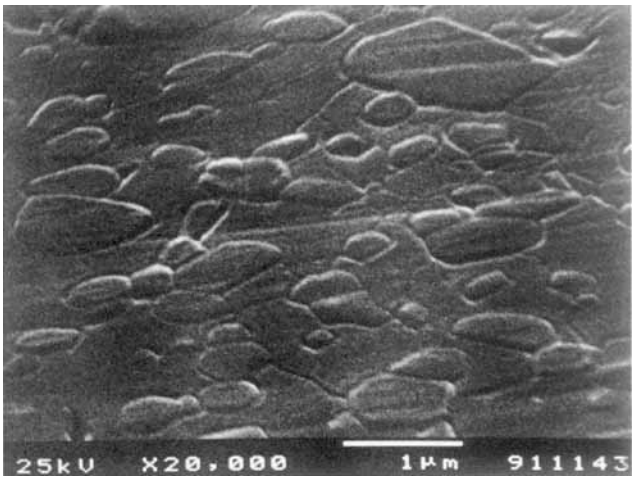

Fig. 14. SEM micrograph of polished and thermally etched Al_2O_3–15SiC(C) composite first oxidized at 1300°C for 5 h and followed by a 1600°C sintering for 2 h in Ar.

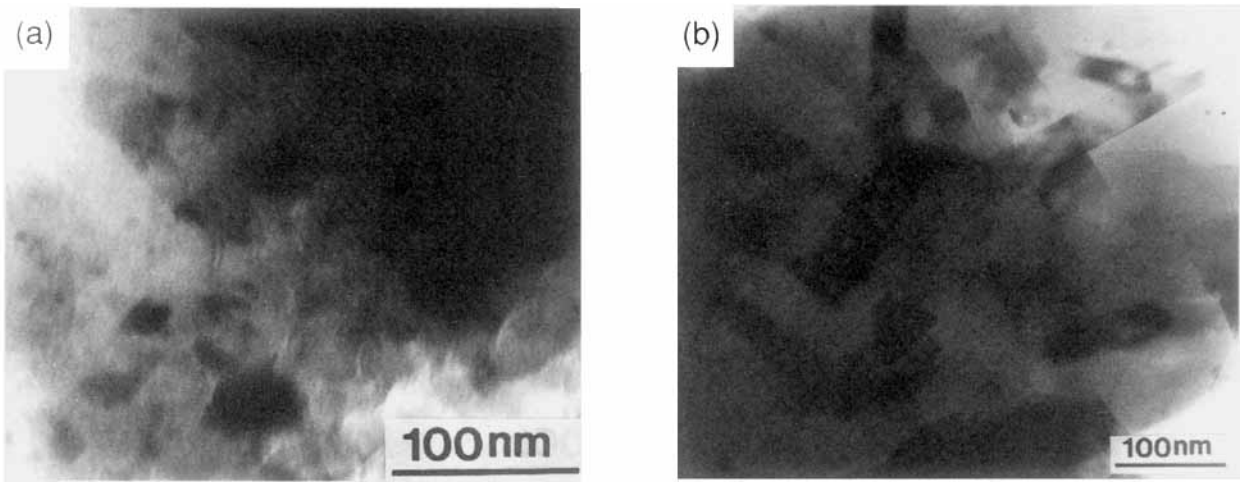

Fig. 15. TEM micrographs of (a) Al_2O_3–15SiC(F) and (b) Al_2O_3–15SiC(C) composites first oxidized at 1300°C for 5 h in air and followed by a final sintering treatment at 1600°C for 2 h in Ar.

that result in preferential oxidation into the SiC grains, producing the type of microstructure observed in Fig. 15(b) by the mechanism summarized below.

Recent studies have shown that in the temperature range <1500°C, mullite forms by a nucleation and growth process within the silica-rich matrix (but not at the alumina interfaces) as the siliceous matrix is saturated with respect to mullite through the dissolution of alumina.[34–36] In this process, first, Al_2O_3 dissolves into the amorphous silica matrix; second, mullite nuclei form within this matrix as the matrix composition exceeds the saturation limit with respect to mullite; and third, mullite crystals grow as more alumina dissolves into the matrix and then is incorporated into the growing mullite grains. The nucleation and growth of mullite within silica-rich fissures on the coarse SiC would then be consistent with the morphology observed in Fig. 15(b).

IV. Conclusions

SiC–mullite–Al_2O_3 nanocomposites were processed through a novel colloidal consolidation and reaction sintering process. First, micrometer-sized SiC and Al_2O_3 particles were colloidally dispersed and consolidated to form uniformly mixed compacts. Second, the SiC particles were partially oxidized to reduce them to nanometer-sized cores. Third, these nanometer-sized core particles were trapped within a mullite matrix as the silica oxidation product reacted with alumina to form mullite.

This process offers several advantages and thereby warrants further research: (1) it eliminates the need to reduce the particle size of the inclusion phase to the nanometer range by milling and thus provides better control in minimizing impurities; and (2) because of a volume increase during reaction sintering, sintering shrinkages are lower.

Acknowledgments: The main part of this work was conducted in the Department of Materials Science and Engineering, University of Washington, Seattle, WA. We acknowledge M. Sarikaya and J. Liu of the University of Washington, and T. Uchikoshi of NRIM, for their help with the TEM observations. We also wish to thank Otsuka Electrics and Bel Japan, Inc., for measuring the electrophoretic mobility.

References

[1]R. P. Andres, R. S. Averback, W. L. Brown, W. A. Goddard III, A. Kaldor, S. G. Louie, M. Moscovits, P. S. Peercy, S. J. Riley, R. W. Siegel, F. Spaepen, and Y. Wang, "Research Opportunities on Cluster and Cluster-Assembled Materials," *J. Mater. Res.*, **4** [3] 705–36 (1989).

[2]R. W. Siegel, R. Ramasamy, H. Hahn, L. Tiang, and R. Gronsky, "Synthesis, Characterization, and Properties of Nanophase TiO_2," *J. Mater. Res.*, **3**, 1367–72 (1988).

[3]K. Niihara, "New Design Concepts of Structural Ceramics—Ceramic Nanocomposite," *J. Ceram. Soc. Jpn.*, **99** [10] 974–82 (1991).

[4]H. Takada, A. Nakahira, H. Ohnishi, S. Ueda, and K. Niihara, "Improvement of Mechanical Properties of Natural Mullite/SiC Nanocomposite," *Jpn. J. Powder Powder Met.*, **38**, 348–51 (1991).

[5]T. N. Tiegs, P. F. Becher, and P. Angelini, "Microstructure and Properties of SiC Whisker-Reinforced Mullite Composite"; pp. 463–72 in Ceramic Transactions, Vol. 6, *Mullite and Mullite Matrix Composites*. Edited by S. Somiya, R. F. Davis, and J. A. Pask. American Ceramic Society, Westerville, OH, 1990.

[6]B. R. Marple and D. J. Green, "Mullite/Alumina Particulate Composites by Infiltration Processing: III, Mechanical Properties," *J. Am. Ceram. Soc.*, **74** [10] 2453–59 (1991).

[7]Y. Sakka, D. D. Bidinger, J. Liu, M. Sarikaya, and I. A. Aksay, "Processing of SiC–Mullite–Al_2O_3 Nanocomposite"; pp. 15–26 in NASA Conference Publication, Vol. 3175, *The 16th Conference on Metal Matrix, Carbon, and Ceramic Matrix Composites*. Edited by J. D. Buckley. National Aeronautics and Space Administration, Washington, DC, 1992.

[8]I. A. Aksay, F. F. Lange, and B. I. Davis, "Uniformity of Al_2O_3–ZrO_2 Composites by Colloidal Filtration," *J. Am. Ceram. Soc.*, **60** [10] C-190–C-192 (1983).

[9]F. F. Lange, "Powder Processing Science and Technology for Increased Reliability," *J. Am. Ceram. Soc.*, **72** [1] 3–15 (1989).

[10]S. Ross and I. D. Morrion, *Colloidal Systems and Interfaces*; pp. 205–63. Wiley, New York, 1988.

[11]C. Han, "Sintering of Bimodal Powder Compacts"; M.S. Thesis. University of California, Los Angeles, CA, 1985.

[12]C. Han, I. A. Aksay, and O. J. Whittemore, "Characterization of Microstructure Evolution with Mercury Porosimetry"; pp. 339–47 in *Advances in Materials Characterization, II*. Edited by R. L. Snyder, R. A. Condrate, Sr., and P. F. Johnson. Plenum, New York, 1985.

[13]E. Liden, L. Bergstrom, M. Persson, and R. Carlsson, "Surface Modification and Dispersion of Silicon Nitride and Silicon Carbide Powders," *J. Eur. Ceram. Soc.*, **7** [6] 361–68 (1990).

[14]J. Cesarano III, I. A. Aksay, and A. Bleier, "Stability of Aqueous α-Al_2O_3 Suspensions with Poly(methacrylic acid) Polyelectrolyte," *J. Am. Ceram. Soc.*, **71** [4] 250–55 (1988).

[15]J. Cesarano III and I. A. Aksay, "Processing of Highly Concentrated Aqueous α-Al_2O_3 Suspensions Stabilized with Polyelectrolytes," *J. Am. Ceram. Soc.*, **71** [12] 1062–67 (1988).

[16]Y. Hirata and I. A. Aksay, "Particle Segregation during Colloidal Filtration"; pp. 3–15 in *Advances in Materials, Processing and Manufacturing, Proceedings of the Advanced Materials Technology Ceramic Workshop*, No. 4. International Committee for Advanced Materials Technology, Nagoya, Japan, 1988.

[17]J. Liu, W. Y. Shih, R. Kikuchi, and I. A. Aksay, "Clustering of Binary Colloidal Suspensions: Theory," *J. Colloid Interface Sci.*, **142** [2] 369–77 (1991).

[18]M. Yasrebi, W. Y. Shih, and I. A. Aksay, "Clustering of Binary Colloidal Suspensions: Experiment," *J. Colloid Interface Sci.*, **142** [2] 357–68 (1991).

[19]M. D. Sacks and G. W. Scheiffele, "Properties of Silicon Suspensions and Slip-Cast Bodies," *Ceram. Eng. Sci. Proc.*, **6** [7–8] 1109–23 (1985).

[20]Y. Sakka, T. Uchikoshi, and E. Ozawa, "Low-Temperature Sintering and Gas Desorption of Gold Ultrafine Powders," *J. Less-Common Met.*, **147**, 89–96 (1989).

[21]Y. Sakka, S. Ohno, and M. Uda, "Oxidation and Degradation of Titanium Nitride Ultrafine Powders Exposed to Air," *J. Am. Ceram. Soc.*, **75** [1] 244–48 (1992).

[22]W. L. Vaughn and H. G. Maahs, "Active-to-Passive Transition in the Oxidation of Silicon Carbide and Silicon Nitride in Air," *J. Am. Ceram. Soc.*, **73** [6] 1540–43 (1990).

[23]G. Ervin, Jr., "Oxidation Behavior of Silicon Carbide," *J. Am. Ceram. Soc.*, **41** [9] 347–52 (1958).

[24]P. J. Jorgensen, M. E. Wadsworth, and I. B. Cutler, "Oxidation of Silicon Carbide," *J. Am. Ceram. Soc.*, **42** [12] 613–16 (1959).

[25]R. F. Adamsky, "Oxidation of Silicon Carbide in the Temperature Range 1200 to 1500°," *J. Phys. Chem.*, **63**, 305–7 (1959).
[26]K. L. Luthra, "Some New Perspectives on Oxidation of Silicon Carbide and Silicon Nitride," *J. Am. Ceram. Soc.*, **74** [5] 1095–103 (1991).
[27]T. Shimoo, "Carbon Removal and Oxidation of SiC Powder Synthesized by Carbothermic Reduction of Silica," *J. Ceram. Soc. Jpn.*, **99** [9] 768–73 (1991).
[28]W. Jander, "Reactions in Solid State at High Temperatures: I," *Z. Anorg. Allg. Chem.*, **163**, 1 (1927).
[29]E. W. Sucov, "Diffusion of Oxygen in Vitreous Silica," *J. Am. Ceram. Soc.*, **46** [1] 14–20 (1963).
[30]F. J. Norton, "Permeation of Gaseous Oxygen Through Vitreous Silica," *Nature (London)*, **191**, 4789 (1961).
[31]S. Wu and N. Claussen, "Fabrication and Properties of Low-Shrinkage Reaction-Bonded Mullite," *J. Am. Ceram. Soc.*, **74** (10] 2460–63 (1991).
[32]M. D. Sacks, N. Bozkurt, and G. W. Scheiffele, "Fabrication of Mullite-Matrix Composites by Transient Viscous Sintering of Composite Powders," *J. Am. Ceram. Soc.*, **74** [10] 2428–37 (1991).
[33]J. E. Webb, "Processing Mullite for Use as a Ceramic–Ceramic Composite Matrix Material"; M.S. Thesis. University of Washington, Seattle, WA, 1991.
[34]S. Sundaresan and I. A. Aksay, "Mullitization of Diphasic Aluminosilicate Gels," *J. Am. Ceram. Soc.*, **74** [10] 2388–92 (1991).
[35]W. Wei and J. W. Halloran, "Transformation Kinetics of Diphasic Aluminosilicate Gels," *J. Am. Ceram. Soc.*, **71** [7] 581–87 (1988).
[36]J. C. Huling and G. L. Messing, "Epitactic Nucleation of Spinel in Aluminosilicate Gels and Its Effect on Mullite Crystallization," *J. Am. Ceram. Soc.*, **74** [10] 2374–81 (1991). □